Weierstraß-Institut

für Angewandte Analysis und Stochastik

im Forschungsverbund Berlin e. V.

Preprint ISSN 0946 – 8633

Hysteresis and Phase Transition in Many-particle Storage Systems

Wolfgang Dreyer[1], Clemens Guhlke[1], Michael Herrmann[2]

submitted: 2nd February 2010

[1] Weierstrass-Institute
for Applied Analysis
and Stochastics
Mohrenstr. 39
10117 Berlin
Germany
E-Mail: dreyer@wias-berlin.de
guhlke@wias-berlin.de

[2] University of Oxford
Mathematical Institute
24-29 St Giles
Oxford OX1 3LB
England
E-Mail: michal.herrmann@maths.ox.ac.uk

No. 1481
Berlin 2010

2000 *Mathematics Subject Classification.* 35Q84, 80A22, 74N30.

2010 *Physics and Astronomy Classification Scheme.* 05.10.Gg,05.70.Fh, 05.70.Ce, 82.47.Aa.

Key words and phrases. thermodynamics, phase transitions, hysteresis, many particle system, Focker-Planck equation, lithium-ion batteries, rubber balloons.

Edited by
Weierstraß-Institut für Angewandte Analysis und Stochastik (WIAS)
Mohrenstraße 39
10117 Berlin
Germany

Fax: +49 30 2044975
E-Mail: preprint@wias-berlin.de
World Wide Web: http://www.wias-berlin.de/

Abstract

We study the behavior of systems that can be described as ensembles of interconnected storage particles. Our examples concern the storage of lithium in many-particle electrodes of rechargeable lithium-ion batteries and the storage of air in a system of interconnected rubber balloons. We are particularly interested in those storage systems whose constituents exhibit non-monotone material behavior leading to transitions between two coexisting phases and to hysteresis. In the current study we consider the case that the time to approach equilibrium of a single storage particle is much smaller than the time for full charging of the ensemble. In this regime, the evolution of the probability to find a particle of the ensemble in a certain state may be described by a nonlocal conservation law of Fokker-Planck type. The resulting equation contains two parameter which control whether the ensemble transits the 2-phase region along a Maxwell line or along a hysteresis path, or whether the ensemble shows the same non-monotone behavior as its constituents.

1 Introduction

Reversible storage systems are of key importance in modern energy technologies. They serve to store electrical or chemical energy for later use, in particular in mobile applications. In this study we consider storage systems that consist of an ensemble of many interconnected storage particles. The technological applications concern ensembles of nano-sized crystalline solids, where matter is stored on lattice sites. Modern many-particle electrodes of lithium-ion batteries belong to this class of storage systems. The storage of hydrogen in certain metals provides a further example.

Our first goal is to develop a generic model that is capable of simulating the evolution of many-particle storage systems during slow loading respectively unloading. We apply this model to $FePO_4$ electrodes of lithium-ion batteries. Moreover, in order to illustrate the crucial behavior of many particle systems we also consider a macroscopic system of interconnected rubber balloons. Such a system may serve to store air and exhibits a similar behavior as the ensemble of nano-sized $FePO_4$ particles.

Rechargeable lithium-ion batteries are the most promising storage devices to store and convert chemical energy into electrical energy and vice versa [1]. The basic functionality of a lithium-ion battery relies on the system anode-cathode-electrolyte-separator. We focus on electrodes that consist of a powder of 10^{10} - 10^{17} nano-particles on a substrate. These nano-particles serve to store lithium atoms reversibly, and the electrode acts as a cathode during the discharging of the battery. For modelling and simulation we consider a half cell consisting of a many-particle Li_yFePO_4 electrode against metallic Li within an electrolyte of infinite conductivity. The storage particles of a fully discharged battery consists of $LiFePO_4$, i.e. in this state the lithium mole fraction of a storage particle is $y = 1$, whereas we have $y = 0$ in the fully charged battery.

During discharging of the battery, the interstitial lattice sites of the $FePO_4$ crystal are filled up with lithium atoms and these are released again during charging. These processes are accompanied by quite large mechanical deformations, because the lithium atoms need more space than it is available by the interstitial lattice sites, leading to a maximal relative change of the crystal volume of about 6%.

The characteristics of charging and discharging of a lithium-ion battery is represented in the voltage-capacity diagram. In the half cell, the voltage U is related to a mean chemical potential, $\langle\mu\rangle$, by

$$U = -\frac{\langle\mu\rangle}{e_0} + U_0. \tag{1}$$

The quantity $\langle\mu\rangle$ will be defined below and calculated within the model, e_0 denotes the electric charge of an electron, and U_0 is the cell voltage. The capacity is proportional to the contained charge of the cell and the charge is proportional to $1 - q$, where q represents the filling degree of the $FePO_4$ particles, i.e. the total amount of stored lithium.

The Figure 1 shows the typical behavior of the half cell. The time for full charging is 20 hours and hence very large with respect to the diffusional relaxation time of a single storage particle, which is about 1 second. The voltage-capacity diagram reveals two

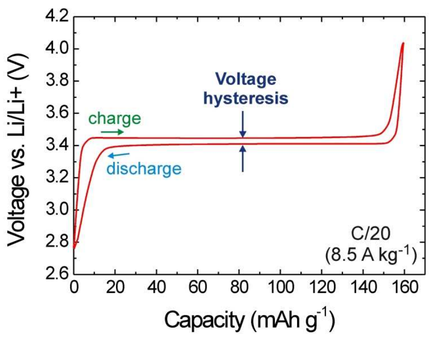

Figure 1: Voltage versus capacity of a $FePO_4$ half cell [6].

crucial phenomena. We observe hysteretic behavior and horizontal branches, indicating a phase transition in the many-particle system during charging and discharging. The main objective of this study is the simulation of the voltage-capacity diagram and to explain the origin of the two phenomena.

Classically hysteresis may be related to variations of charging rate, particles size, electrode thickness etc. In this context we mention the electrode systems TiO_2 [10],

$LiFeSiO_4$ [19], $LiCoO_2$ [13] and $LiFePO_4$ [27]. These mechanisms are called *classical* because they lead to a decrease of the overvoltage by decreasing the current density or by increasing the impedance due to charge transport. However, there is a further non-classical hysteresis inducing phenomenon, that was first observed for the $LiFePO_4$ electrode by M. Gaberšček et al. [6]. At a first glance it should be expected that the overvoltage due to classical hysteretic effects should tend to zero for decreasing current, whereas the $LiFePO_4$ electrode exhibits a finite voltage gap for zero current. We will show that this kind of hysteresis is induced by the configurational entropy of a many-particle system and appears only for slow loading when there is sufficient time to exchange lithium atoms between the storage particles.

The second characteristic property of many-particle electrodes is a phase transition during loading-unloading processes and we now summarize the ongoing debate on this matter. Based on experimental studies of Li_yFePO_4 bulk matter, Yamada et al. [27] suggest that in a certain region of the total lithium mole fraction y two phases coexist. These phases are called α- and β-phase, and correspond to high and low lithium mole fraction, respectievly. The horizontal branches from Figure 1 indicate that the same phenomenon also occurs in a system of nano-sized Li_yFePO_4 particles. In fact, it was assumed that there is likewise a 2-phase region in the single particle, and the simplest model setting is the *core-shell model* that was first suggested by Padhi et. al. [20]: In the 2-phase region a single spherical storage particle consists of an inner core and an outer shell. The core-shell model is established and applied to the process of insertion and extraction of lithium by Srinivasan and Newman [22, 23] within a sharp interface model. Moreover, Ceder et al. [9] formulate and exploit a phase field model of Cahn-Hilliard type, and Dreyer et. al. [4] use the core-shell model to take the coupling of diffusional and mechanical phenomena into account. In [26] Wagemaker et. al. study various different morphologies of a 2-phase system within a single storage particle.

However, careful studies on the coexistence of two phases within a single storage particle recently gave rise to some doubts concerning the stability of two coexisting phases. Wagemaker et al. [24] investigated for lithiated anatase TiO_2 the dependence of the phase diagram on the particle size. If the particles become too small, the formation of two phases is energetically unfavorable due to the high interfacial energy between the different intercalated phases. Corresponding experiments with $LiFePO_4$ by Delmas and his group [2] lead to similar results. They report that even in larger particles two coexisting phases can not be observed. Instead Delmas et al. observe homogeneous particles that are either in the high or in the low lithium mole fraction phase. Thus the horizontal branches cannot explained anymore by two coexisting phases within the single particles. Moreover, Delmas and his group established the *domino cascade model* whereupon the charging/discharging process proceeds sequentially, i.e. particle-by-particle or in other words: one after the other.

In collaboration with J. Jamnik, J. Moškon and M. Gaberšček from the *National Institute of Chemistry Slovenia* who carried out new experiments, we establish in [5] and [6] the *many-particle model* to explain and simulate both the voltage-charge diagram from Figure 1 and the finite hysteresis gap for zero current from Figure 2.

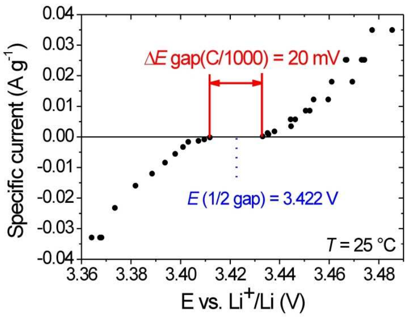

Figure 2: Current versus voltage at charge state of 80mAhg^{-1} of a $FePO_4$ half-cell [6].

The many-particle model considers an electrode consisting of N interconnected $FePO_4$ storage particles for insertion and removal of lithium atoms. It relies on three essential assumptions:

1. The chemical potential of lithium in Li_yFePO_4 , is given by a non-monotone function of y. 2. The charging-discharging rate of a many-particle ensemble is small with respect to the diffusional relaxation time of a single particle. 3. On this slow time scale the lithium distribution is homogeneous within each particle.

The first assumption is motivated by the observed miscibility gap in experiments with Li_yFePO_4 bulk matter. Relying on estimates from [9], the diffusional relaxation time of nano-particles is of the order 1 s, but the usual charging times are currently much larger than this value. The third assumption on the homogeneity of the lithium distribution inside the storage particles is intimately related to a stability problem. Relying on a preliminary study, we conjecture that the 2-phase region of a single storage particle is unstable due to the high interfacial energy between two adjacent phases, so that there is a rapid transition through that region. Therefore, on the slow time scale of charging/discharging we expect that all particles are homogenous. This explains, in particular, why Delmas et al. [2] only observed homogenous particles and no particles with two phases. Between two subsequent observations of the morphologies of the particles in the Delmas experiment there is sufficient time for relaxation of the particles.

However, if the loading time of a many-particle electrode is comparable with the diffusional relaxation time of a single particle, then the coexistence of two phases within a single particle becomes observable and the many-particle model with homogeneous storage particles becomes inadequate. This situation will be studied in a forthcoming paper.

The many-particle electrode has a nice analogon represented by a system of interconnected spherical rubber balloons that can be loaded with air via a pressure vessel. The two systems evolve in a similar way because in correspondence to the many-particle electrode, the pressure difference across the balloon membrane is given by a non-monotone function of the balloon radius. For this reason also the rubber balloon system exhibits phase transitions and hysteresis during the loading-unloading process.

In their paper on rate independent hysteresis from 2001, Truskinovski and Puglisi [21] studied a closely related subject with the objective to explain hysteretic phenomena in shape memory alloys on a microscopic basis. The microscopic model consists of a one-dimensional chain of N oscillators with a non-monotone stress-strain characteristic that intimately corresponds to the non-monotone chemical potential- lithium mole fraction characteristic. Differences of the two studies concern the prescribed side conditions during the cycling of the hysteresis loop and the modelling of the evolution law, see also Mielke and Truskinovski [15]. In order to reduce the necessary assumptions that are needed in a quasi-static treatment of the problem, the authors establish an evolution law, that provides the oscillators in addition to the non-monotone stress-strain characteristic with viscous elements and stochastic behavior. Compared to this strategy, our approach is quite simple as it relies on the configurational entropy.

The analysis of a many particle system, where each particle is equipped with unstable states between two stable states, has been started already in 1982, when Dreyer, Müller, and Strehlow [7] investigated the equilibria of two connected spherical rubber balloons. This problem was later generalized to $N > 2$ connected balloons by Kitsche [11, 12], whose results are in complete analogy to [21] and our findings.

The paper is organized as follows:

In Chapter 2 we develop a general setting to describe the evolution of a generic storage systems that consists of a large number of storage particles whose thermodynamic states are described by a single variable $\xi(t)$. In the limiting case of infinitely many particles we introduce a probability density $w(t,\xi)$ to find at time t a storage particle in the state ξ. For given filling degree $q(t)$ of the ensemble, the evolution law for $w(t,\xi)$ turns out to be a non-local and non-linear Fokker-Planck equation.

Chapters 3 and 6 address the constitutive theory for two applications:

1 The storage problem for a many-particle electrode of a rechargeable lithium-ion battery. Here we focus on $FePO_4$ storage particles and describe their material behavior within the simplified setting of homogeneous particles. In particular we ignore the orthorhombic olivine crystal symmetry. In this case the thermodynamic behavior of a single storage particle is described by a non-monotone chemical potential function that depends only on the lithium mole fraction of the particle.

2 A system of interconnected spherical rubber balloon that serves to store air supplied from a pressure vessel. The analogy to the many-particle electrode results from the fact that the pressure difference across the balloon membrane depends on the strain in a non-monotone manner.

In Chapters 4 and 7 we apply the generic storage model to the two applications and identify the statistical variable as the lithium mole fraction of a single storage particle in the battery case, and as the strain of a single rubber balloon in the second example. The evolution equations for both storage systems are then described in Chapters 5 and 8.

In Chapter 9 we present detailed numerical simulations for a many-particle electrode during loading and unloading. In Chapter 10 we then compare simulations of the rubber balloon systems with experimental results.

2 General model of many-particle storage systems

2.1 Evolution of Energy and Entropy in an Open System

In what follows we consider a generic system Ω with volume V that may exchange heat, mechanical work and matter with the environment via its surface $\partial\Omega$. We assume that $\partial\Omega = \partial\Omega_{\mathrm{m}} \cup \partial\Omega_{\mathrm{ex}}$, where $\partial\Omega_{\mathrm{m}}$ denotes a material part which is subjected to a constant pressure p_0. $\partial\Omega_{\mathrm{ex}}$, however, is not material but allows the transfer of matter equipped with the enthalpy per molecule h_{ex} at a rate dN_{ex}/dt, where N_{ex} gives the number of stored molecules at time t. The energy E of Ω evolves according to the conservation law of energy, which reads

$$\frac{dE}{dt} = \dot{Q} - p_0\frac{dV}{dt} + h_{\mathrm{ex}}\frac{dN_{\mathrm{ex}}}{dt} \ . \tag{2}$$

Next we assume that the temperature T is constant in $\Omega \cup \partial\Omega$, and this can be guaranteed by choosing an appropriate heat power $\dot{Q}$. Under this assumption the entropy S of Ω satisfies the inequality

$$\frac{dS}{dt} \geq \frac{\dot{Q}}{T} + s_{\mathrm{ex}}\frac{dN_{\mathrm{ex}}}{dt} \ , \tag{3}$$

where s_{ex} abbreviates the entropy per molecule of the supplied matter. Of course, in equilibrium we have an equality sign in (3). More details about the fundamental laws (2) and (3) and can be found in the textbook [17].

2.2 The fundamental inequality for isothermal processes

By combination of (2) and (3) we may eliminate the heat power $\dot{Q}$ to obtain the fundamental thermodynamic inequality for isothermal processes

$$\frac{d\mathscr{A}}{dt} \leq g_{\mathrm{ex}}\frac{dN_{\mathrm{ex}}}{dt} \quad \text{with} \quad \mathscr{A} = E - TS + p_0 V \quad \text{and} \quad g_{\mathrm{ex}} = h_{\mathrm{ex}} - Ts_{\mathrm{ex}} \ . \tag{4}$$

The quantity $\mathscr{A}$ represents the total free energy of the system and $\Psi = E - TS$ denotes its Helmholtz free energy including the kinetic energy, which, however, will be ignored in this study. The Gibbs free energy per particle of the incoming matter is abbreviated by g_{ex}. The Helmholtz free energy is a constitutive quantity that will be explicitly calculated from the constitutive models for the two cases at hand in Chapters 3 and 6. Later on we will exclusively study processes with prescribed rate dN_{ex}/dt, and in this case g_{ex} must be determined within the model.

2.3 General representation of the total free energy

The storage particles of the ensemble are indexed by $l \in \{1, 2, ..., N\}$. Their essential properties are embodied by two assumptions: (i) The particles are homogeneous on the time scale of slow charging of the storage system. (ii) The thermodynamic state of any particle l is sufficiently described by a single time dependent function $\xi_l(t) \in [a, b]$.

The homogeneity assumption restricts the model to slow charging, recall the detailed discussion in the Introduction and see [6]. The description of a particle by a single variable, viz. ξ, relies on the fact that mechanical equilibrium is established at any instant of time. In this case we can solve the mechanical problem in advance, so that we can eliminate the mechanical variables as functions of ξ. The fundamental inequality (4) then reflects that the ensemble approaches the phase equilibrium during the processes of charging and discharging. Moreover, due to the second assumption, the free energy of particle l can be represented by a function $A_l = A(\xi_l)$, where we restrict to the case that each particle is described by the same function A.

The total free energy of the storage system has two contributions. The first one is the sum of the free energies of the particles, and the second one is the configurational entropy, which takes care of the interchange of matter between the storage particles due to fluctuations. We write

$$\mathscr{A} = \sum_{l=1}^{N} A(\xi_l) - TS_{\text{conf}}. \tag{5}$$

As a preparation to calculate S_{conf} we decompose the interval $[a, b]$ into N subintervals indexed by $\alpha \in \{1, 2, ..., N\}$ of length $(b-a)/N$, and denote by Z_α the number of particles of the ensemble with states in the subinterval $i_\alpha = [\xi_\alpha, \xi_{\alpha+1}]$. In order to control the amount of stored molecules we introduce the filling degree of the storage system by $q \equiv N_{\text{ex}}/(N\bar{\mathscr{N}})$, where $\bar{\mathscr{N}}$ denotes a constant characteristic particle number of the system. In this setting we now characterize a thermodynamic state of an ensemble with N storage particles by the sequence $\{Z_1, Z_2, ..., Z_N\}$ that satisfies the conditions

$$1 = \frac{1}{N} \sum_{\alpha=1}^{N} Z_\alpha, \quad \text{and} \quad q = \frac{1}{N} \sum_{\alpha=1}^{N} G(\xi_\alpha) Z_\alpha, \tag{6}$$

where $G(\xi_\alpha)$ is related to the number of stored molecules in the subinterval i_α and will be specified below.

Due to fluctuations the interconnected storage particles exchange the stored molecules, so that a given sequence $\{Z_1, Z_2, ..., Z_N\}$ can be realized in many ways. The number R of realizations is calculated according to

$$R = \frac{N!}{Z_1!Z_2!...Z_N!}, \tag{7}$$

and the configurational entropy follows from Boltzmann's formula $S = k\log R$, where k denotes the Boltzmann constant.

After rearranging the $A(\xi_l)$'s in (5) and using Stirling's formula for large numbers we obtain a general representation the total free energy of the ensemble

$$\mathscr{A} = \sum_{\alpha=1}^{N} A(\xi_\alpha)Z_\alpha + kT \sum_{\alpha=1}^{N} Z_\alpha \log\big(\frac{Z_\alpha}{N}\big) \ . \tag{8}$$

We divide (8) by NE_0, where E_0 is a constant energy to be chosen below, and set $F = A/E_0$, $\nu^2 = kT/E_0$, and substitute $\mathscr{A}/(NE_0) \to \mathscr{A}$. This gives

$$\mathscr{A} = \frac{1}{N}\sum_{\alpha=1}^{N} F(\xi_\alpha)Z_\alpha + \nu^2\frac{1}{N} \sum_{\alpha=1}^{N} Z_\alpha \log\big(\frac{Z_\alpha}{N}\big) \ . \tag{9}$$

The probability W_α to find a storage particle in the subinterval i_α is given by $W_\alpha = Z_\alpha/N$ and its density w_α is defined by $W_\alpha = w_\alpha\Delta\xi_\alpha = w_\alpha \cdot (b-a)/N$. Hence we have $Z_\alpha = Nw_\alpha\Delta\xi_\alpha$. We now pass to the limit $N \to \infty$ and substitute $w_\alpha \to w(t,\xi)$. The free energy of the whole storage system can then be written as

$$\mathscr{A}(t) = \int_a^b \big(F(\xi) + \nu^2 \log w(t,\xi)\big)\, w(t,\xi)\, d\xi \ . \tag{10}$$

2.4 The evolution of the probability density

In this section we derive an evolution equation for the probability density $w(t,\xi) \geq 0$. This equation must satisfy the fundamental inequality (4) as well as the two side conditions (6). With $\Lambda = (g_{\text{ex}}\bar{\mathscr{N}})/E_0$ these read in the continuous setting

$$\frac{d\mathscr{A}}{dt} - \Lambda\frac{dq}{dt} \leq 0, \quad 1 = \int_a^b w(t,\xi)d\xi, \quad q(t) = \int_a^b G(\xi)w(t,\xi)d\xi \ . \tag{11}$$

Now we insert the mean values (10) and $(11)_3$ into the inequality and obtain

$$\int_a^b \Big(F(\xi) - \Lambda(t)G(\xi) + \nu^2\big(1 + \log w(t,\xi)\big)\Big)\frac{\partial w(t,\xi)}{\partial t}\, d\xi \leq 0 \ . \tag{12}$$

In order to satisfy the normalization condition $(11)_2$ as well as the positivity condition $w \geq 0$ we assume that $w(t,\xi)$ satisfies a conservation law of the type

$$\frac{\partial w(t,\xi)}{\partial t} + \frac{\partial \upsilon(t,\xi)w(t,\xi)}{\partial \xi} = 0 \tag{13}$$

with boundary conditions $\upsilon(t,a)w(t,a) = \upsilon(t,b)w(t,b) = 0$. We now determine the velocity function $\upsilon(t,\xi)$ such that the inequality (12) is satisfied. To this end we eliminate the time derivative in (12) by means of (13), and using integration by parts we find

$$\int_a^b \Big(\big(F'(\xi) - \Lambda(t)G'(\xi)\big) + \nu^2 \frac{\partial \log(w(t,\xi))}{\partial \xi}\Big)\upsilon\, w(t,\xi)\; d\xi \leq 0\;. \tag{14}$$

The simplest possibility to satisfy the inequality (14) is obviously given by

$$\tau\upsilon = \big(\Lambda G'(\xi) - F'(\xi)\big) - \nu^2 \frac{\partial \log(w(t,\xi))}{\partial \xi}\;, \tag{15}$$

where $\tau > 0$ is a positive phenomenological constant, which can be interpreted as the relaxation time of the ensemble.

Finally, combining (13) and (15) gives the desired evolution equation for the probability density $w(t,\xi)$. It reads

$$\tau \frac{\partial w(t,\xi)}{\partial t} + \frac{\partial}{\partial \xi}\Big(\big(\Lambda(t)G'(\xi) - F'(\xi)\big)w(t,\xi)\Big) = \nu^2 \frac{\partial^2 w(t,\xi)}{\partial \xi^2} \tag{16}$$

and fits into the the class of Fokker-Planck equations.

It remains to guarantee the side condition $(11)_3$ for a prescribed charging rate, i.e. to determine the unknown function $\Lambda(t)$. At first we use a generic function $m(\xi)$ to introduce the mean value

$$\langle m\rangle(t) = \int_a^b m(\xi)w(t,\xi)d\xi. \tag{17}$$

Then we multiply (16) by $m(\xi)$ and integrate with respect to ξ. This gives

$$\tau \frac{d\langle m\rangle}{dt} - \Lambda\langle G'm'\rangle + \langle F'm'\rangle = \nu^2\langle m''\rangle - \nu^2\big(m'(b)w(b) - m'(a)w(a)\big)\;. \tag{18}$$

The special choice $m = G$ leads to the following relation between the charging rate and the unknown function $\Lambda(t)$

$$\tau\dot{q} - \Lambda\langle G'G'\rangle + \langle F'G'\rangle = \nu^2\langle G''\rangle - \nu^2\big(G'(b)w(b) - G'(a)w(a)\big)\;, \tag{19}$$

which can be solved for $\Lambda(t)$.

2.5 Summary of the general model

We propose a general model of a storage system that consists of an ensemble of many interconnected storage particles. The thermodynamic state of a single storage particle is described by a single variable $\xi \in [a,b]$. Any particle of the ensemble is equipped with a free energy function $F(\xi)$. The prescribed mean number of stored molecules in a particle is represented by the mean value of a given function $G(\xi)$. The statistical behavior of the ensemble is represented by a probability density $w(t,\xi) \geq 0$, whose initial- and boundary value problem reads

$$
\begin{aligned}
& w(0,\xi) = w_0(\xi), \qquad \upsilon(t,a)w(t,a) = \upsilon(t,b)w(t,b) = 0, \\
& \frac{\partial w(t,\xi)}{\partial t} + \frac{\partial \upsilon(t,\xi)w(t,\xi)}{\partial \xi} = 0, \\
& \tau\upsilon(t,\xi) = \big(\Lambda(t)G'(\xi) - F'(\xi)\big) - \nu^2 \frac{\partial \log(w(t,\xi))}{\partial \xi} \,.
\end{aligned}
\tag{20}
$$

The problem is non-local and non-linear because the function $\Lambda(t)$ must be calculated from (19).

By means of the general model we will study now a many-particle electrode of a rechargeable lithium-ion battery and for illustration we consider a system of rubber balloons that behaves similar. It will turn out that the properties of the model are simply controlled by the two constant parameter τ and ν^2 that both have an intuitive meaning.

3 Constitutive model 1: Many-particle electrode of a lithium-ion battery

3.1 General properties of many-particle electrode material

We study the electrode of rechargeable lithium-ion batteries that acts as a cathode during discharging of the battery, Figure 3. In modern batteries the cathode consists of a powder of 10^{10} - 10^{17} nano-particles on a substrate. Here we consider $FePO_4$ particles which have orthorhombic olivine symmetry. There is a sublattice whose sites may be empty or occupied by lithium atoms. To each unit of $FePO_4$ there corresponds one single site in the sublattice. The sublattice of the fully charged battery is empty whereas the storage particles consist of $LiFePO_4$ in the complete discharged state of the battery.

3.2 Thermodynamic state of a storage particle

On the time scale of experiments with an ensemble of storage particle, which is much larger than the diffusional relaxation time of a single nano-particle, only homogeneous particles have been observed, see [2, 24]. This fact motivates the essential assumption of the thermodynamics in this paper: The particles are assumed to be homogeneous.

The number $\mathcal{N}_{\mathrm{M}}$ of $FePO_4$ units, which form the matrix lattice, is fixed. On the sublattice of a particle we have $\mathcal{N}_{\mathrm{Li}}$ lithium atoms and $\mathcal{N}_{\mathrm{V}}$ empty sites which we call

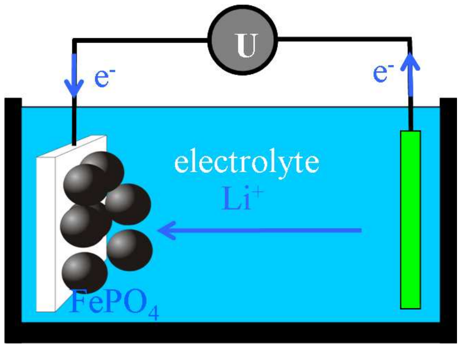

Figure 3: Half cell with many-particle electrode.

vacancies. These do not have mass or momentum but they are carrier of energy and entropy. Since there is a single sublattice site to each $FePO_4$ unit, we have the side condition

$$\mathcal{N}_{\mathrm{M}} = \mathcal{N}_{\mathrm{Li}} + \mathcal{N}_{\mathrm{V}}. \tag{21}$$

Thus for given temperature T, the basic variables of a storage particle are its volume V and the mole numbers $\mathcal{N}_{\mathrm{M}}$ and $\mathcal{N}_{\mathrm{Li}}$. For the local description we introduce the mole densities n_{M}, n_{Li} and n_{V} which have units $\mathrm{mole}/\mathrm{m}^3$. Note that n_{M} changes because the volume V may change, whereas $\mathcal{N}_{\mathrm{M}}$ is constant.

Further quantities, which are related to the basic variables, are the mass density ρ with $\rho = m_{\mathrm{M}} n_{\mathrm{M}} + m_{\mathrm{Li}} n_{\mathrm{Li}} = n_{\mathrm{M}}(m_{\mathrm{M}} + m_{\mathrm{Li}} y)$, where m_{M} and m_{Li} are the molecular masses of $FePO_4$ and Li, respectively, and $y = n_{\mathrm{Li}}/n_{\mathrm{M}}$ gives the lithium mole fraction.

3.3 Free energy density, chemical potentials, pressure, Gibbs equation and Gibbs-Duhem equation

We denote the free energy density of a storage particle by $\rho\psi$, where ψ is the specific free energy.

The specific free energy is given by a constitutive function that relates ψ to the temperature T, which is a constant here, and to the mole densities n_{Li}, n_{V} of lithium and vacancies. Since we have $n_{\mathrm{M}} = n_{\mathrm{Li}} + n_{\mathrm{V}}$, we may change variables from n_{Li}, n_{V} to y, n_{M}:

$$\psi = \psi(T, n_{\mathrm{Li}}, n_{\mathrm{V}}) = \tilde{\psi}(T, y, n_M). \tag{22}$$

The free energy density satisfies the Gibbs equation and the Gibbs-Duhem equation, see [3] and [16]. These read

$$d\rho\psi = -\rho s dT + \sum_{a\in(\mathrm{Li},\mathrm{V})} \mu_a dn_a \quad \text{and} \quad p = -\rho\psi + \sum_{a\in(\mathrm{Li},\mathrm{V})} \mu_a n_a, \tag{23}$$

where the newly introduced quantities are the entropy density ρs, the chemical potentials μ_a and the pressure p. From (23) and by an direct calculation we obtain the relations

$$\mu_a = \frac{\partial \rho \psi}{\partial n_a} , \quad \mu_{\mathrm{Li}} - \mu_{\mathrm{V}} = m_{\mathrm{Li}} \tilde{\psi} + (m_{\mathrm{M}} + m_{\mathrm{Li}} y) \frac{\partial \tilde{\psi}}{\partial y} , \quad p = -\rho \tilde{\psi} + n_{\mathrm{M}} \frac{\partial \rho \tilde{\psi}}{\partial n_{\mathrm{M}}} . \tag{24}$$

3.4 Explicit constitutive equations

The explicit knowledge of the specific free energy allows to calculate the chemical potentials and the pressure. Our strategy to determine the specific free energy, i.e. $\psi = \psi(T, n_{\mathrm{Li}}, n_{\mathrm{V}}) = \tilde{\psi}(T, y, n_{\mathrm{M}})$, relies on the observation that we may additively decompose $\rho\psi$ into a chemical and a mechanical part, i.e.,

$$\rho\psi = \rho\tilde{\psi}^{\mathrm{chem}}(T, y, n_{\mathrm{M}}) + \rho\tilde{\psi}^{\mathrm{mech}}(T, y, n_{\mathrm{M}}) \quad \text{with} \quad \tilde{\psi}^{\mathrm{mech}}(T, y = 0, \bar{n}_{\mathrm{M}}) = 0. \tag{25}$$

The constant $\bar{n}_{\mathrm{M}}$ denotes the matrix density in a reference state that refers to an empty $FePO_4$ particle.

Chemical part of the free energy. In this study we use the same non-convex constitutive law as in [4, 9], which takes into account both the configurational entropy and the heat of solution. We write

$$\rho\tilde{\psi}^{\mathrm{chem}} = n_{\mathrm{M}} L\, f^{\mathrm{chem}}(y) \tag{26}$$

with

$$f^{\mathrm{chem}}(y) = y(1-y) + \frac{RT}{L}(y \log y + (1-y) \log(1-y)), \tag{27}$$

where $L > 0$ is the constant heat of solution, and $R > 0$ denotes the universal gas constant.

Mechanical part of the free energy. The details of the mechanical properties of the crystal Li_yFePO_4 are investigated by T. Maxisch and G. Ceder [14]. In [4] we discuss the complete mechanical part of the free energy for the olivine crystal symmetry of Li_yFePO_4. Here, however, we only account for volume changes of the storage particle. Note that the maximal variation of the crystal volume between $FePO_4$ and $LiFePO_4$ is up to 6%.

The mechanical part of the free energy density of the particles is represented by

$$\rho\tilde{\psi}^{\mathrm{mech}} = n_{\mathrm{M}} L\, f^{\mathrm{mech}}(y, n_{\mathrm{M}}) \tag{28}$$

with

$$f^{\mathrm{mech}}(y, n_{\mathrm{M}}) = \frac{p_{\mathrm{R}} - K h(y)}{L} \left(\frac{1}{\bar{n}_{\mathrm{M}} h(y)} - \frac{1}{n_{\mathrm{M}}} \right) + \frac{K}{L \bar{n}_{\mathrm{M}}} \log\left(\frac{n_{\mathrm{M}}}{\bar{n}_{\mathrm{M}} h(y)} \right). \tag{29}$$

This leads to a linear law between the pressure and the relative volume change, which can be described by the function $h(y) = 1/(1+\delta y)$ with a constant $\delta > 0$. Therefore we have

$$p = \bar{p} + K\big(\frac{n_{\mathrm{M}}}{\bar{n}_{\mathrm{M}}} - h(y)\big) . \tag{30}$$

The pressure $\bar{p}$ describes the reference state and the quantity K denotes a mean bulk modulus of Li_yFePO_4.

3.5 Mechanical equilibrium of a many-particle electrode

In comparison with the processes that drive the many-particle ensemble to phase equilibrium, the mechanical equilibrium of the system is much faster established. For this reason it is reasonable to assume that the storage system is in mechanical equilibrium at any time. This assumption allows to reduce the free energy density of particle $l \in 1, 2, ..., N$ to a function of a single variable.

Recall that the surrounding of the N particles is under the constant pressure p_0. In this simplified setting, the mechanical equilibrium is then described by the N conditions

$$p(y^l, n^l_{\mathrm{M}}) = p_0 \quad \text{implying} \quad n^l_{\mathrm{M}} = \hat{n}_{\mathrm{M}}(y^l) = \bar{n}_{\mathrm{M}} \left(h(y^l) + \frac{p_0 - \bar{p}}{K} \right) . \tag{31}$$

The function $\hat{n}_{\mathrm{M}}(y^l)$ can now be used to eliminate the mole densities n^l_{M}. Thus the free energy functions $\psi^l = \tilde{\psi}(y^l, n_{\mathrm{M}})$ become functions of a single variable and are represented by $\psi(y^l) = \tilde{\psi}(y^l, \hat{n}_{\mathrm{M}}(y^l))$.

4 The total free energy of a many-particle electrode

We consider the many-particle electrode as indicated in Figure 3. Relying on the constitutive model for $\mathrm{Li}_y\mathrm{FePO}_4$ storage particles from the previous chapter we identify the generic statistical variable ξ with the lithium mole fraction, i.e., we set $\xi = y$ for $y \in [0, 1]$.

In order to give an explicit representation of the total free energy $\mathscr{A}$ of the ensemble we start from the general formulas (5),(8) and (10). Recall that $A(y^l) = V^l(\rho\psi^l + p_0)$ represents the single particle energy of particle l and V^l is its volume. The constitutive function A can be simplified by two further assumptions:

(i) The number constants $\mathscr{N}^l_{\mathrm{M}}$ of matrix molecules (FePO_4) are the same for each storage particle $\mathscr{N}^l_{\mathrm{M}} = \mathscr{N}^1_{\mathrm{M}}, l = 1, \ldots, N$.

(ii) All particles have the same volume $\bar{V}$ in the unloaded state, implying that they have the same mole density $\bar{n}_{\mathrm{M}}$.

Thus we obtain $A(y^l) = \bar{n}_{\mathrm{M}}\bar{V}\ (\rho\psi^l + p_0)/n^l_{\mathrm{M}}$. The total total free energy $\mathscr{A}$ and the free energy $A(y^l)$ of the particle l will be scaled by $E_0 = \bar{n}_{\mathrm{M}}\bar{V}L$, compare the derivation of (10).

Finally we use the formulas from Section 3.4 to assemble the total free energy. This yields the explicit form of the function $F(y)$ from (10) and the constant $\nu^2 = kT/(\bar{n}_{\mathrm{M}}\bar{V}L)$. The total free energy of the many-particle electrode finally reads

$$\mathscr{A}(t) = \int_a^b \big(F(y) + \nu^2 \log\, w(t,y)\big)\, w(t,y)\,dy \quad \text{with} \tag{32}$$

$$F(y) = f^{\mathrm{chem}}(y) + f^{\mathrm{mech}}(y, \hat{n}_{\mathrm{M}}(y)) + \frac{p_0}{L\hat{n}_{\mathrm{M}}(y)} . \tag{33}$$

For later use in the discussion of the simulations we need the difference $\mu = \mu_{\mathrm{Li}} - \mu_{\mathrm{V}}$ of the chemical potentials of lithium and the vacancies, respectively. An easy but careful calculation yields

$$\mu(y) = \mu_{\mathrm{Li}}(y, \hat{n}_{\mathrm{M}}(y)) - \mu_{\mathrm{V}}(y, \hat{n}_{\mathrm{M}}(y)) = \frac{dF}{dy} \,. \tag{34}$$

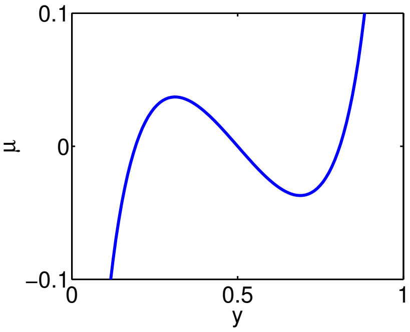

Figure 4: Chemical potential difference according to (34).

5 The evolution of a many-particle electrode

The evolution equation for the probability density $w(t,y)$ of a many-particle electrode stems from the generic problem (20). In order to prescribe the processes of loading respectively unloading, we introduce the macroscopic filling degree defined by $q = \mathscr{N}_{\mathrm{Li}}/\mathscr{N}_{\mathrm{M}}$. Then, the generic function $G(y)$ turns out to be $G(y) = y$, so we have

$$q(t) = \int_0^1 y w(t,y) dy \,. \tag{35}$$

Consequently, for given filling degree $q(t)$ the evolution of a many-particle electrode is governed by

$$\begin{aligned}
&w(0,y) = w_0(y), \qquad \upsilon(t,0)w(t,0) = \upsilon(t,1)w(t,1) = 0, \\
&\frac{\partial w(t,y)}{\partial t} + \frac{\partial \upsilon(t,y)w(t,y)}{\partial y} = 0, \\
&\tau\upsilon(t,y) = \Lambda(t) - \mu(y) - \nu^2 \frac{\partial \log(w(t,y))}{\partial y} \,.
\end{aligned} \tag{36}$$

Recall that this PDE is non-local and non-linear as the function $\Lambda(t)$ must be determined from the side condition (35) by means of (19).

In (36) there appear two constant parameter: τ is the relaxation time of the storage system, and ν^2 measures the importance of the configurational entropy of the ensemble. Note that ν^2 decreases if the size of the particles increases.

6 Constitutive model 2: A system of interconnected rubber balloons

6.1 General properties of a system of interconnected rubber balloons

We study a system of N spherical rubber balloons that are connected via a pressure vessel as is indicated in Figure 5. The system may be loaded or onloaded with air and we are interested in the evolution of the balloons. There is a strong similarity between the described many-particle electrode of a lithium-ion battery and a system of interconnected balloons. Recall that the chemical potential μ of a single storage particle is given by a non-monotone function of the lithium mole fraction. On the other hand, the relation between the pressure difference across a spherical rubber balloon versus the balloon filling is a non-monotone function. For this reason the ensemble of interconnected balloons shows the same type of phase transition and hysteresis as the many-particle electrode.

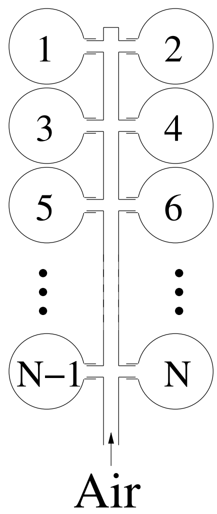

Figure 5: System of a pressure vessel and interconnected rubber balloons

6.2 Thermodynamic state of an air filled spherical rubber balloon

We denote the radii of the deformed respectively undeformed balloon by r and R. The radial strain λ of the balloon is then defined by $\lambda = r/R$. The air molecules with molecular mass m_A in the balloon are assumed to be homogenously distributed and their actual number is denoted by $\mathscr{N}$. The number of air molecules in the undeformed reference state is $\bar{\mathscr{N}}$. We consider processes at constant temperature $T = \bar{T}$ and characterize a thermodynamic state of the system *balloon plus air* by the variables λ and $\mathscr{N}$. The volume V of the balloon may be related to the strain by $V = \bar{V}\lambda^3$ with

$\bar{V} = 4\pi R^3/3$. The mole density of air molecules is denoted by $n_\mathrm{A} = \mathcal{N}/V$ and has the unit mole/m^3.

6.3 Free energy densities, pressures and Gibbs equations

The system *balloon plus air* is described by two free energy densities: 1. The free energy density of air, denoted by $(\rho\psi)_\mathrm{A}$, where ψ_A is the specific free energy of air and ρ_A denotes its mass density. 2. The free energy density $(\rho\psi)_\mathrm{B}$ of a spherical balloon is decomposed into the specific free energy ψ_B of a rubber membrane and the mass per surface area ρ_B.

The corresponding constitutive functions have the forms

$$\psi_\mathrm{A} = \hat{\psi}_\mathrm{A}(T, n_\mathrm{A}), \quad \text{and} \quad \psi_\mathrm{B} = \hat{\psi}_\mathrm{B}(T, \lambda) \; . \tag{37}$$

As above, the free energy densities satisfy the Gibbs equation which read for an air filled rubber balloon:

$$d\psi_\mathrm{A} = -s_\mathrm{A} dT - \frac{p_\mathrm{A}}{m_\mathrm{A}} d\frac{1}{n_\mathrm{A}} \quad \text{and} \quad d\psi_\mathrm{B} = -s_\mathrm{B} dT - \frac{1}{\rho_\mathrm{B}} P dr \; . \tag{38}$$

Here s_A and s_B denote the specific entropies, p_A is the air pressure, and P is related to the surface stress of the balloon. Concerning the general setting of surface thermodynamics and the precise definition of surface stress we refer the reader to [7, 18, 8].

6.4 Explicit constitutive equations

The explicit knowledge of the specific free energies allows to calculate the air pressure p_A and the surface stress P of a spherical rubber balloon.

Free energy density of air. The air is assumed to be a 2-atomic ideal gas. In this case its free energy density is represented by the function

$$(\rho\psi)_\mathrm{A}(T, n_\mathrm{A}) = n_\mathrm{A} kT \log\left(\frac{n_\mathrm{A}}{\bar{n}_\mathrm{A}}\right) + (\rho\psi)_\mathrm{A}(T, \bar{n}_\mathrm{A}) \; , \tag{39}$$

leading to the gas pressure $p_\mathrm{A} = n_\mathrm{A} kT$.

Free energy density of a rubber balloon. Rubber is isotropic and incompressible and its mechanical properties are here described by a Mooney Rivlin constitutive law for the free energy density. For more details about the mechanical properties of rubber and rubber balloons we refer to [7, 18]. In what follows we consider a spherical balloon of thin thickness, so that the membrane limit can be applied. Up to terms of 2$^\mathrm{nd}$ order in the reference thickness $\bar{d}$, the free energy per surface area is represented by

$$(\rho\psi)_\mathrm{B}(T, \lambda) = \frac{1}{2}\bar{d}\left(s_+(2+\lambda^{-6}) - s_-(\lambda^2 + 2\lambda^{-4})\right) \; , \tag{40}$$

where the Mooney-Rivlin constants depend on temperature. At 40°C they have values $s_+ = 30\text{N/cm}^2$ and $s_- = -0.1s_+$.

6.5 Mechanical equilibrium of a system of air filled interconnected rubber balloons

We assume that mechanical equilibrium across the balloon membrane is much faster established than mechanical equilibrium of the air in the balloon system. This assumption allows to reduce the free energy density of balloon $l \in \{1,2,\ldots,N\}$ and the contained air to a function of a single variable.

Mechanical equilibrium between the membrane and the innner pressure p_l is given by, see [7, 18],

$$p_l - p_0 = P(\lambda_l) \ , \tag{41}$$

where the non-monotone function

$$P(\lambda_l) = \frac{2\bar{d}}{R}\left(s_+(\lambda_l^{-1} - \lambda_l^{-7}) - s_-(\lambda_l^{1} - \lambda_l^{-5})\right) \ , \tag{42}$$

follows from $(38)_2$ and (40), and is sketched in the first diagram of Figure 6.

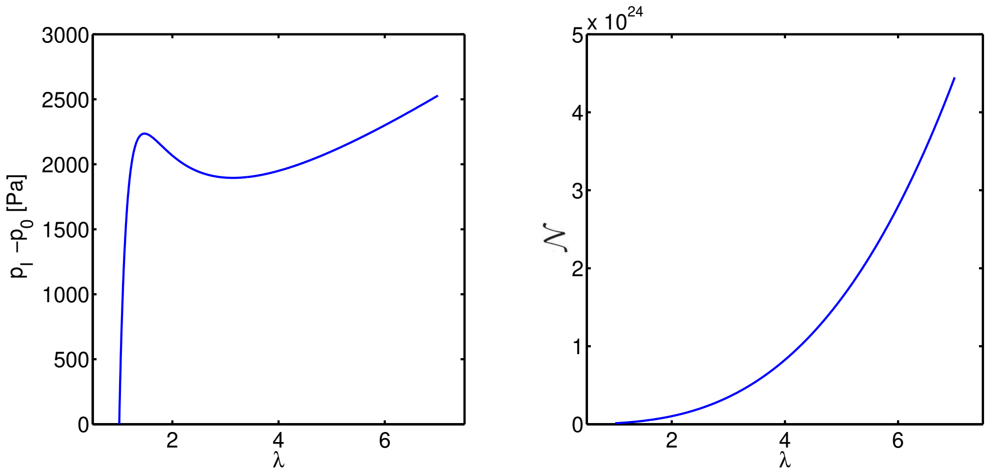

Figure 6: Left: Equilibrium pressure jump across a single balloon versus strain λ. Right: Number of air molecules contained in a single balloon versus its strain λ.

We insert the gas pressure into (41) and obtain a relation between the number of contained air molecules $\mathcal{N}_l$ and the strain λ_l of the balloon $l \in \{1,2,\ldots,N\}$:

$$\mathcal{N}_l = \hat{\mathcal{N}}(\lambda_l) = \frac{V_l}{kT}p_l = \bar{\mathcal{N}}\lambda_l^3\left(1 + \frac{P(\lambda_l)}{p_0}\right) \ . \tag{43}$$

The second diagram of Figure 6 reveals that this dependence is monotone in contrast to the pressure-strain relation (41). The function $\hat{\mathcal{N}}(\lambda_l)$ may now be used to eliminate the number of air molecules $\mathcal{N}_l$ as variables.

7 The total free energy of a rubber balloon system

Relying on the constitutive model for the rubber balloon system from the previous chapter, we identify the generic statistical variable ξ with the radial strain: $\xi = \lambda$ for $\lambda \in [1, \lambda^*]$.

In order to give an explicit representation of the total total free energy $\mathscr{A}$ of the system we start from the general form which is represented by (5),(8),(10). The free energy of a single balloon is given by

$$A(\lambda_l) = \bar{V} \left(\lambda_l^3 \left((\rho\psi)_{\mathrm{A}}^l + p_0 \right) + \frac{3}{R} \lambda_l^2 (\rho\psi)_{\mathrm{B}}^l \right) , \tag{44}$$

and both A and $\mathscr{A}$ will in turn be scaled by $E_0 = p_0 \bar{V}$.

Finally we calculate the free energy densities from (39) and (40) and identify the generic function $F(\lambda)$ from (10) and the constant $\nu^2 = kT/(p_0\bar{V}) = \bar{\mathscr{N}}^{-1}$. The total free energy of the rubber balloon system hence reads

$$\mathscr{A}(t) = \int_1^{\lambda^*} \left(F(\lambda) + \nu^2 \log w(t,\lambda) \right) w(t,\lambda) d\lambda \quad \text{with} \tag{45}$$

$$\begin{aligned} F &= \frac{\hat{\mathscr{N}}(\lambda)}{\bar{\mathscr{N}}} \left(\log \left(\frac{P(\lambda)}{p_0} \right) - 1 \right) \\ &\quad + \frac{3}{2} \frac{\bar{d}}{R p_0} \left(s_+ (2\lambda^2 + \lambda^{-4}) - s_- (\lambda^4 + 2\lambda^{-2}) \right) + \lambda^3 , \end{aligned} \tag{46}$$

and a direct computation yields

$$\frac{dF}{d\lambda} = \frac{1}{\bar{\mathscr{N}}} \frac{d\hat{\mathscr{N}}}{d\lambda} \log \left(\frac{P(\lambda)}{p_0} \right) . \tag{47}$$

8 The evolution of a rubber balloon system

The evolution equation for the probability density $w(t,\lambda)$ of a rubber balloon system relies on the generic problem (20). In order to prescribe the processes of loading respectively unloading, we introduce the macroscopic filling degree $q = \mathscr{N}/\bar{\mathscr{N}}$ denoting the overall loading state of the system. In this case the generic function $G(\lambda)$ turns out to be $G(\lambda) = \hat{\mathscr{N}}(\lambda)/\bar{\mathscr{N}}$, so we have

$$q(t) = \frac{1}{\bar{\mathscr{N}}} \int_1^{\lambda^*} \hat{\mathscr{N}}(\lambda) w(t,\lambda) d\lambda . \tag{48}$$

For given filling degree $q(t)$ the evolution of the rubber balloon system it thus represented by

$$w(0,\lambda) = w_0(\lambda), \qquad \upsilon(t,1)w(t,1) = \upsilon(t,\lambda^*)w(t,\lambda^*) = 0,$$

$$\frac{\partial w(t,\lambda)}{\partial t} + \frac{\partial \upsilon(t,\lambda)w(t,\lambda)}{\partial \lambda} = 0, \tag{49}$$

$$\tau\upsilon(t,\lambda) = \frac{\hat{\mathscr{N}}'(\lambda)}{\bar{\mathscr{N}}}\left(\Lambda(t) - \log\left(\frac{P(\lambda)}{p_0}\right)\right) - v^2 \frac{\partial \log(w(t,\lambda))}{\partial \lambda}\,.$$

Recall that this PDE is non-local and non-linear as the function $\Lambda(t)$ must be determined from the side condition (48) by means of (19).

As in the lithium case we have two constant parameter: the relaxation time τ of the balloon system and v^2 that measures the configurational entropy effect. Note that increasing the size of the undeformed balloon implies a decreasing v^2.

9 Selected simulations for the many-particle electrode

In this section we prescribe the history of loading-unloading processes by the filling degree $q(t)$ and solve the evolution equation (36) for the probability density $w(t,y)$. In order to separate the chemical from the mechanical phenomena we ignore here changes of the particle volume and set $\delta = 0$ and $p_0 = \bar{p}$. The case where both phenomena are coupled will be discussed in a forthcoming study.

We solve the equation for $y \in [0,1]$ and with boundary conditions $\upsilon(t,0)w(t,0) = \upsilon(t,1)w(t,1) = 0$. Initially we start the simulation in the 1-phase region, where the storage particles are Gaussian distributed around a small value, $q_0 = 0.1$, for the initial filling degree. This reads

$$w(0,y) = w_0(y) = \sqrt{\frac{\mu'(q_0)}{2\pi v^2}}\exp\left(-\frac{\mu'(q_0)}{2v^2}(y-q_0)^2\right)\,. \tag{50}$$

We have performed simulations for 45 different values of (τ, v^2) but with the same loading-unloading path: At first we increase the filling degree q linearly from $q = 0.1$ to $q = 0.9$ and afterwards we decrease it from $q = 0.9$ to $q = 0.1$. The time t has been normalized by $|\dot{q}| = 1$, so the parameter $\tau = \tau_\mathrm{D}/\tau_\mathrm{L}$ gives the ratio between relaxation time τ_D of the storage system and loading time τ_L. In particular, for fixed τ_D a small τ corresponds to a large loading time.

In order to illustrate the typical behavior of solutions to (36), we choose at first $\tau = 10^{-4}, v^2 = 10^{-4}$. Figure 7 shows snapshots of the probability density at 5 different times, where the arrows indicate the direction of the dynamics.

After a certain period the initial single pulse decays into two pulses indicating the transition from single phase states to the coexistence of two phases and back to single

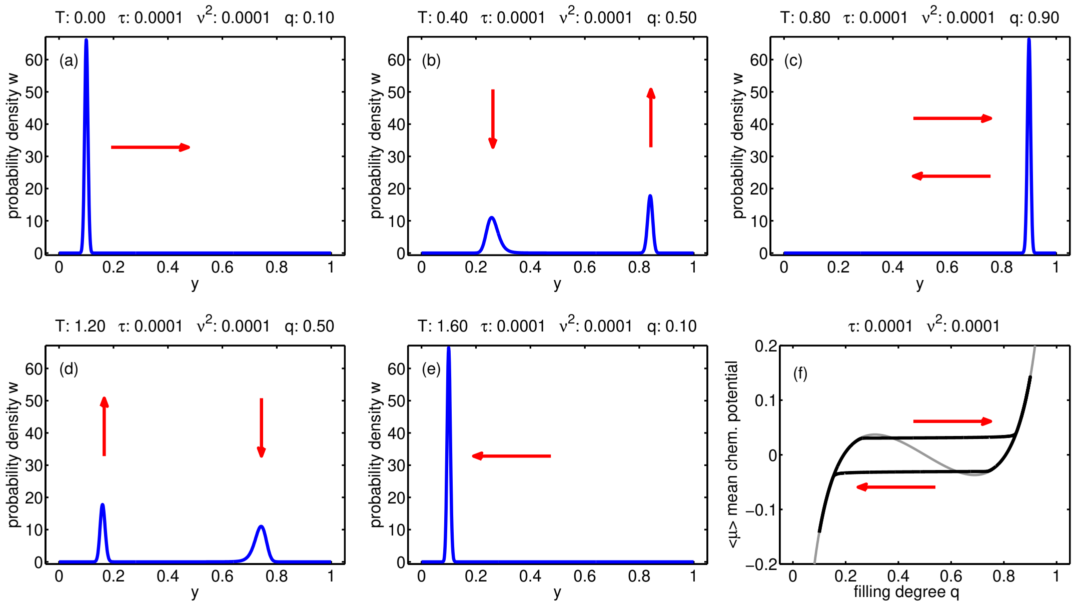

Figure 7: (a)-(e): Evolution of the probability density $w(t,y)$ according a loading-unloading process for $\tau = 10^{-4}$ and $\nu^2 = 10^{-4}$. (f): $(\langle\mu\rangle, q)$ diagram, black: mean chemical potential $\langle\mu\rangle$, gray: chemical potential of single storage particle $\mu(y)$.

phase states for large filling degree. In detail we observe the following dynamics: Initially we have a single pulse, whose maximum is roughly located at $q(t)$ and moves to the right. This behavior changes if the pulse reaches the region where the chemical potential function $\mu(y)$ has negative slope. In that region the initial pulse stops its rightwards motion and a second pulse nucleates at some higher value of the lithium mole fraction y and growths at the expense of the left pulse. The many-particle system runs through a phase transition. After the left pulse has lost all of its mass, the right pulse starts to move rightwards. In that period the system is single-phase again. Finally the filling degree reaches its maximal value and is hereafter reduced. Now the same dynamics happens the other way around.

It is important to observe that the location where a pulse growths or diminishes is different for the loading and the unloading path. This can be seen be comparing Figures $7_{(\mathrm{b})}$ and $7_{(\mathrm{d})}$, which contain corresponding snapshots for the same filling state $q = 0.5$. See also Figure $7_{(\mathrm{f})}$, which contains the $(\langle\mu\rangle, q)$ diagram and reveals how the mean chemical potential $\langle\mu\rangle$ depends on the filling degree q. The path dependence of the process becomes clearly manifest by the hysteresis curve.

Figures 8 and 9 contain the numerical results for $(\tau, \nu) = (0.1, 10^{-5})$ and $(\tau, \nu) = (10^{-5}, 10^{-3})$, respectively, but do not exhibit a hysteretic behavior. In fact, in Figure 8 the many-particle systems behaves like a single particle, whereas the system from Figure 9 follows the Maxwell line.

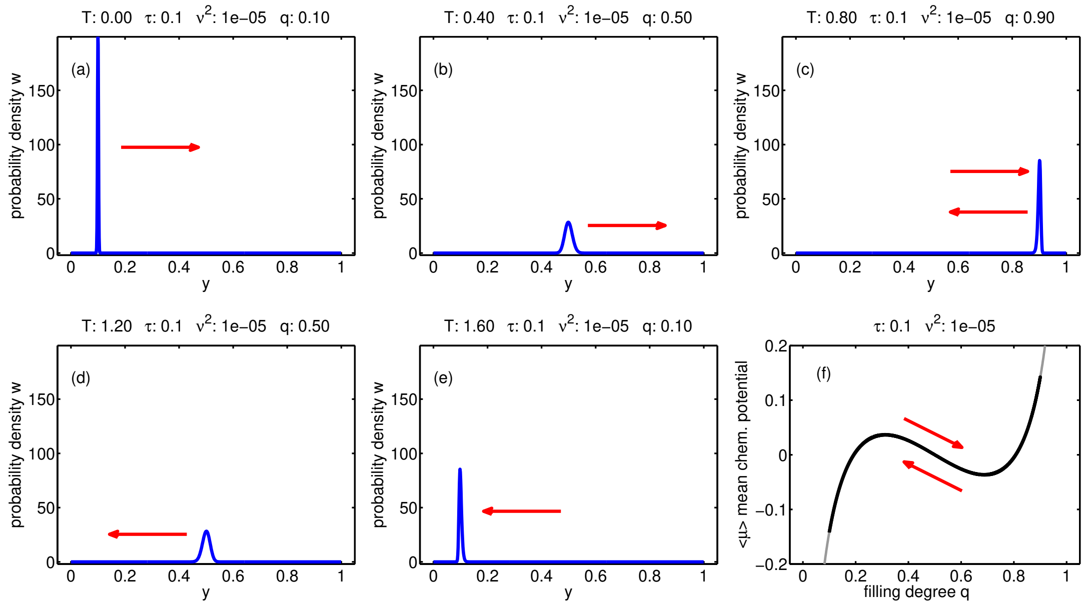

Figure 8: (a)-(e): Evolution of the probability density $w(t,y)$ according a loading-unloading process for $\tau = 0.1$ and $\nu^2 = 10^{-5}$. (f): $(\langle\mu\rangle, q)$ diagram, black: mean chemical potential $\langle\mu\rangle$, gray: chemical potential of single storage particle $\mu(y)$.

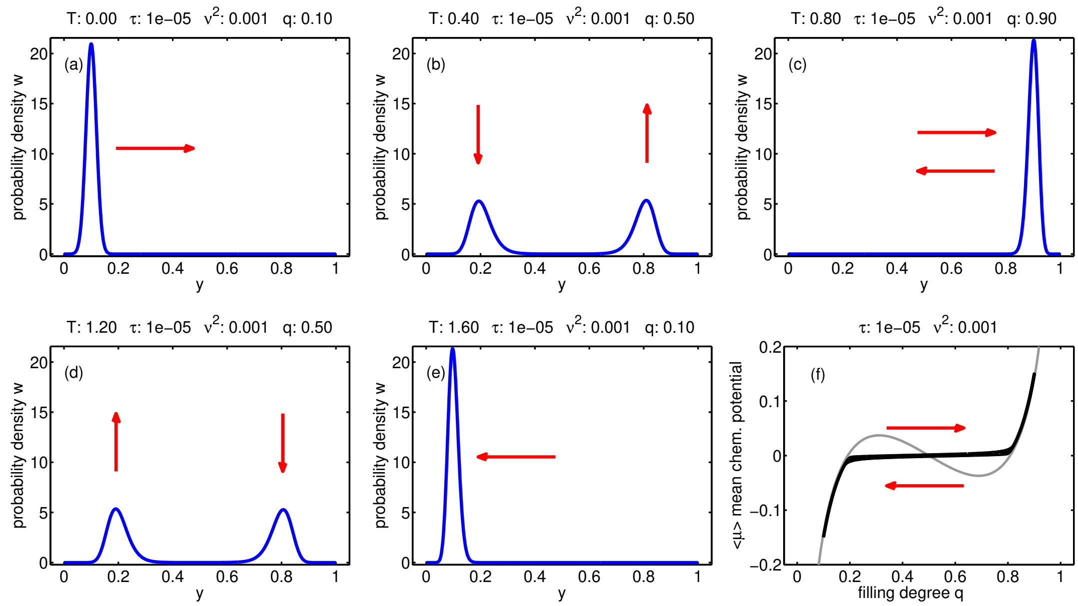

Figure 9: (a)-(e): Evolution of the probability density $w(t,y)$ according a loading-unloading process for $\tau = 10^{-5}$ and $\nu^2 = 10^{-3}$. (f): $(\langle\mu\rangle, q)$ diagram black: mean chemical potential $\langle\mu\rangle$, gray: chemical potential of single storage particle $\mu(y)$.

The location and the shape of the hysteresis is controlled by the two parameter τ and ν^2. This is demonstrated in Table 1, which shows the $(\langle\mu\rangle, q)$ diagrams in a parameter domain that is relevant for applications. The details of the hysteresis curves can be quite involved but we observe three main cases:

1 Case **A**, as in Figure 8: The probability density consists of a single pulse only, because there is not sufficient time to interchange molecules between the storage particles according to the configurational entropy effect. The mean chemical potential follows the chemical potential of a single particle.

2 Case **B**, as in Figure 9: The configurational entropy is dominant and the storage system follows the Maxwell line. A hysteresis does not develop here.

3 Case **C**, as in Figure 7: The deterministic evolution of the system and interchange of molecules due to the configurational entropy are of the same order. A maximal possible hysteresis is developed.

Recall that the value of τ is related to $1/\text{loading time}$, i.e fast and slow loading is represented by small and large τ, respectively. Thus we may interpret the results from Table 1 as follows. The configurational entropy is dominant for very slow loading and drives the storage system along equilibria so that it follows the Maxwell line. The development of hysteresis needs a larger loading time so that the effects of deterministic evolution and interchange of molecules between the storage particles are of equal importance.

In order to classify existing many-particle electrodes according to Table 1 we determine the constants τ and v^2 in applications. We assume that the relaxation time of the system has the same order of magnitude as the diffusional relaxation time of a single storage particle. From [9] we may read off the diffusion constant for the diffusion of lithium in $FePO_4$ viz. 10^{-15}–10^{-17} m^2/s. The loading time of a lithium-ion battery is 10800 s on the average. For particle radii 10–100 nm we obtain τ in the range 10^{-3}–10^{-7} and $v^2 = 10^{-5}$–10^{-8}. The configurational entropy effect is thus comparable with τ, i.e. we meet the case 3. The many-particle electrode passes through the maximal possible hysteresis.

Note that if τ is of order 0.1, the loading time is of order of seconds and the model is not applicable, because the essential assumptions concerning slow loading and homogeneous storage particles are not met in this case.

Table 1: Hysteretic behavior in the $(\langle\mu\rangle, q)$ diagram for severals values of τ and μ. All simulations describe the time evoltuion of the same initial data (50).

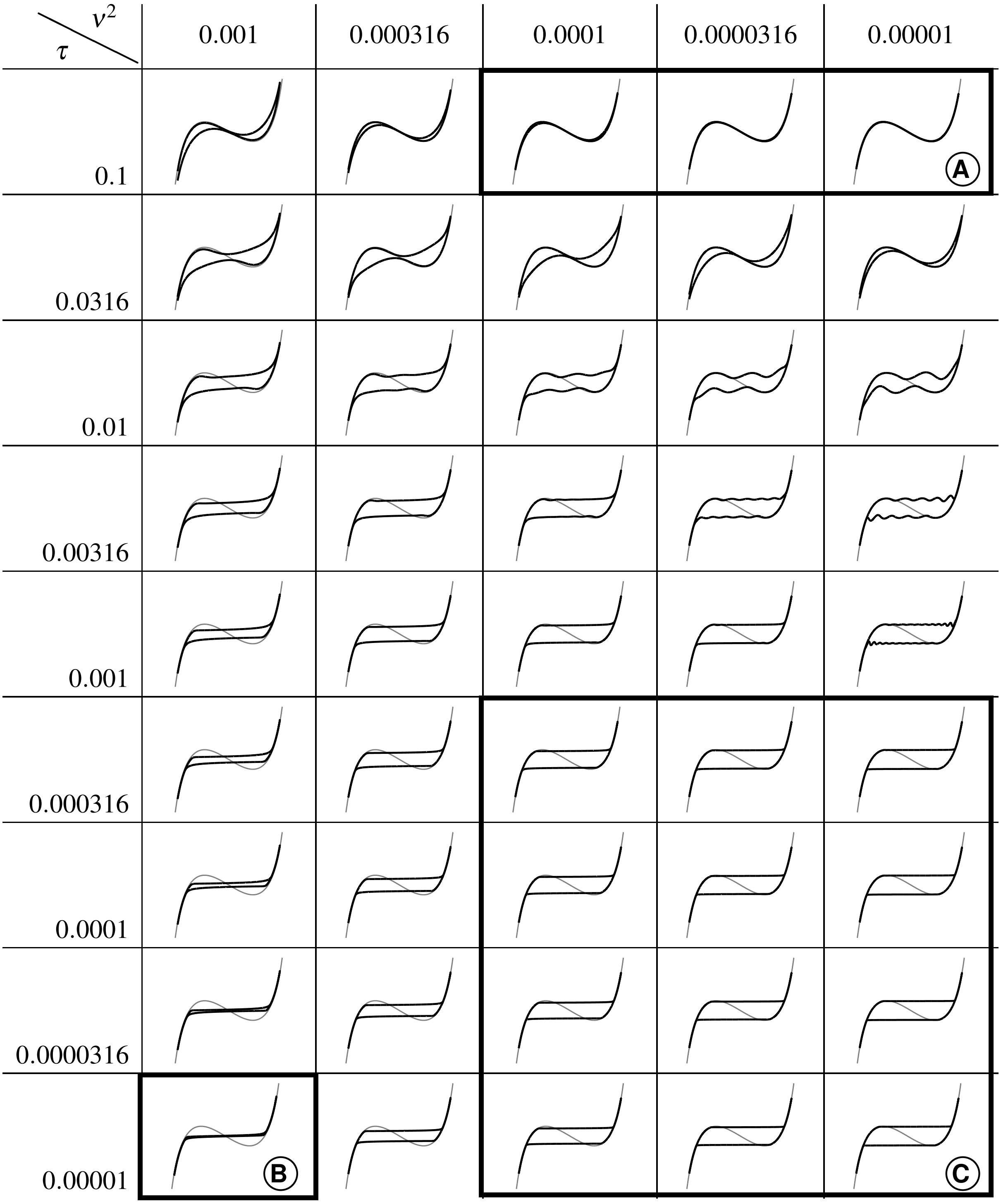

10 Selected simulations for the rubber balloon system

In this section we investigate numerical simulation of the rubber balloon system and compare the numerical outcome with experiments.

The simulations of the Fokker-Planck equation for the many-particle electrode have shown in a certain range of τ and ν^2, the particle system separates into two phases consisting of particles with low and high lithium content. The same phenomenon can be observed in simulations of the rubber balloons system which separates into small and large rubber balloons. Figure 10 shows the evolution of the probability density w for an loading-unloading process und the finial hysteresis. Table 2 then shows the hysteresis in the numerical simulations for different values of (τ, ν) and we observe the same main cases **A**, **B**, and **C** as in Table 1.

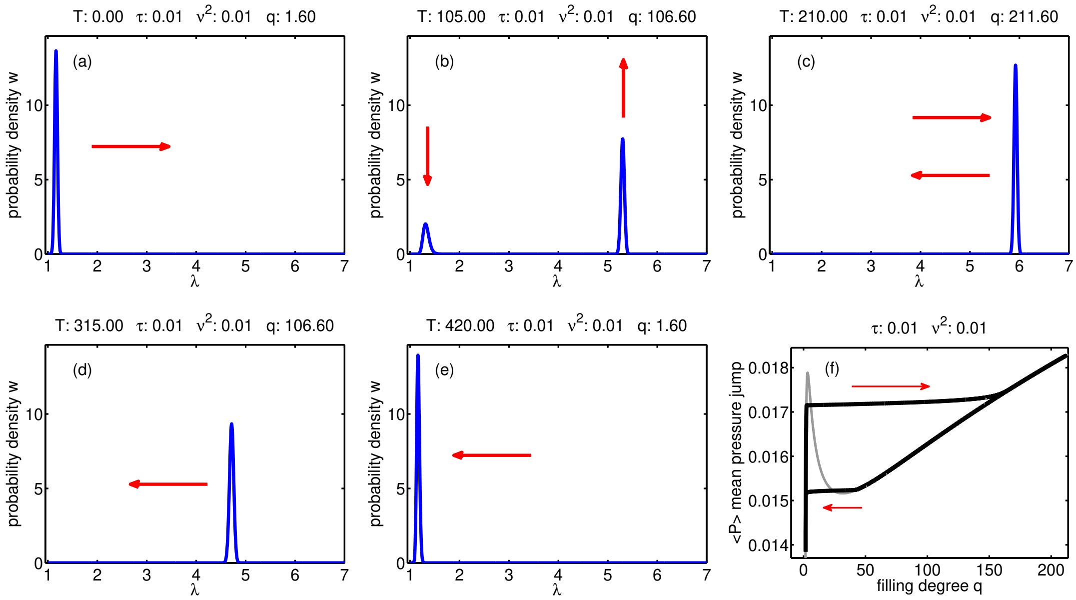

Figure 10: (a)-(e): Evolution of the probability density $w(t, y)$ according a loading-unloading process. (f): Hysteresis, black: mean pressure jump $\langle P \rangle$, gray: pressure jump of single rubber balloon $P(\lambda)$.

Experiments with the rubber balloon system also exhibit the phase separation. The sequence of snapshots in Figure 11 are generated for the analog loading-unloading path as above. Initially we observe only balloons with small filling. After a critical filling degree is reached, the transition to a second phase with large balloons sets in. In this period the balloons grow *one after the other* and we have a system of two coexisting phases with small and large balloons. After the system has reached the single phase states, where only large balloons are present, we unload the balloon system and observe in the 2-phase region that the balloons become smaller according to the same rule as before: *one after the other*.

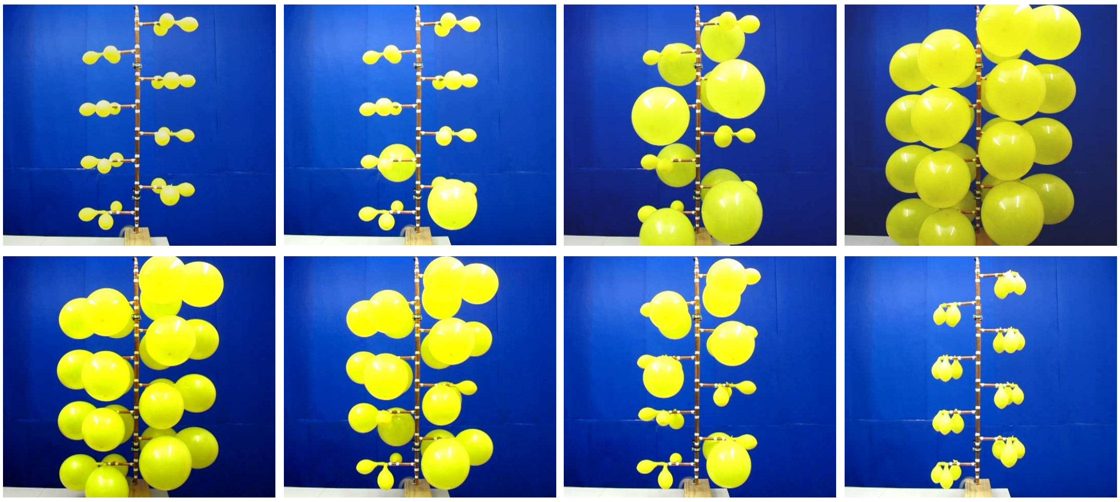

Figure 11: Eight states of interconnected rubber balloons during loading and unloading with air via the pressure vessel.

The simulation of the rubber balloon experiment by means of the application of the corresponding Fokker-Planck equation from Section 8 is very much harder than in the case of the many-particle electrode. This fact is due to the extreme small value of v^2. The characteristic time scale of an air-filled balloon is determined by the sound speed of air, which is about 343 m/s. We take rubber balloons with diameter 0.1 m in the undeformed state, which implies $v^2 = 10^{-22}$. The loading time of the system of balloons is 250 s, which implies $\tau = 10^{-6}$. Thus the configurational entropy effect, which is described by a second order derivative in the Fokker-Planck equation (49), is controlled by an extremely small number so that it is numerically hard to treat. For this reason a careful analysis of the limiting case $v^2 \to 0$ becomes necessary. This, however, is a non-trivial mathematical problem that will be studied in a forthcoming paper.

Table 2: Hysteretic behavior for several values of τ and ν.

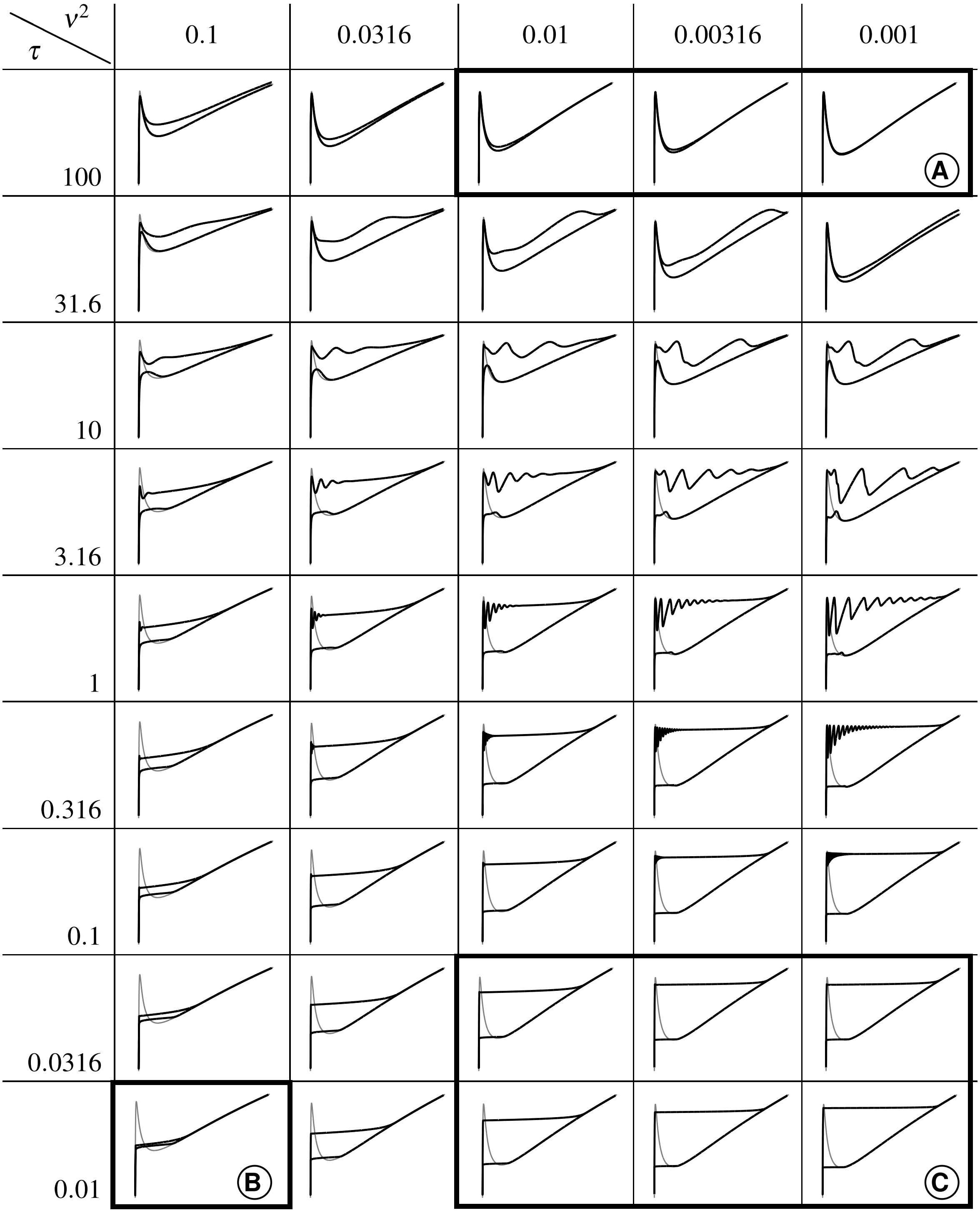

References

[1] M. Armand and J.-M. Tarascon, *Building better batteries*, Nature Vol. **451**, 652–657 (2008).

[2] C. Delmas, M. Maccario, L. Croguennec, F. Le Cras and F. Weill, *Lithium deintercalation in $LiFePO_4$ nanoparticles via a domino-cascade model*, Nature materials, **7** (2008), pp. 665–671.

[3] W. Dreyer and F. Duderstadt, *On the modelling of semi-insulating GaAs including surface tension and bulk stresses*, Proc. R. Soc. Lond. Ser. A Math. Phys. Eng. Sci., 464 (2008) pp. 2693-2720.

[4] W. Dreyer, C. Guhlke, M. Gaberščček, R. Huth and J. Jamnik, *Phase transition and hysteresis in a lithium-ion battery revisited*, Preprint no. 1425, WIAS, Berlin, 2009.

[5] W. Dreyer, C. Guhlke and R. Huth, *The behavior of a many particle cathode in a lithium-ion battery*, WIAS Preprint **1423** (2009).

[6] W. Dreyer, J. Jamnik, C. Guhlke, R. Huth, J. Moškon and M. Gaberščček, *The thermodynamic origin of hysteresis in insertion batteries*, Nature Materials **9** (2010), 448–453.

[7] W. Dreyer, I. Müller and P. Strehlow, *A study of equilibria of interconnected balloons*, Quarterly J. Mech. Appl. **35** (1982), p. 419.

[8] W. Dreyer, *On jump conditions at phase boundaries for ordered and disordered phases*, WIAS-Preprint **869** (2003), p. 419.

[9] B. C. Han, A. Van der Ven, D. Morgan, and G. Ceder, *Electrochemical modeling of intercalation processe with phase field models*, Electrochim. Acta **49** (2004), 4691–4699.

[10] Y.-S. Hu, L. Kienle, Y.-G. Guo and J. Maier *Lithium Electroactivity of Nanometer-Sized Rutile TiO_2*, Adv. Mater. **18** (2006), 1421–1426.

[11] W. Kitsche, *Modellierung eines Phasenüberganges an einem System vieler Ballons*, Diploma thesis, TU Berlin (1985).

[12] W. Kitsche, I. Müller and P. Strehlow, *Simulation of pseudoelastic behavior in a system of rubber balloons*, In: Metastability and incompletely Posed Problems, IMA Vol. **3** (1986), p. 2113.

[13] Levi, M. D., Salitra, G., Markovsky, B., Teller, H., Aurbach, D., Heider, U., Heider, L. *Solid-State Electrochemical Kinetics of Li-Ion Intercalation into LixCoO2: Simultaneous Application of Electroanalytical Techniques SSCV, PITT, and EIS*, J.Electrochem. Soc. **146** (1999), 1279–1289.

[14] T. Maxisch and G. Ceder, *Elastic properties of olivine Li_xFePO_4 from first principles*, Physical Review B **73** (2006), 174112-1–174112-4.

[15] A. Mielke and L. Truskinovsky *Rate-independent plasticity as a double limit: Vanishing viscosity and homogenization*, WIAS-Preprint in preparation (2010).

[16] I. Müller, *Thermodynamics, Interaction of Mechanics and Mathematics Series*, Pitman Advanced Publishing Program, Boston, 1985.

[17] Müller, I. , Müller W. *Fundamentals of Thermodynamics and Applications*, Springer Berlin (2009)

[18] I. Müller and P. Strehlow, *Rubber and Rubber Balloons*, Lecture Notes in Physics **637**, Springer (2004).

[19] Nyten, A., Stjerndahl, M., Rensmo, H., Siegbahn, H., Armand, M., Gustafsson, T., Edstrom, K., Thomas, J. O. *Surface characterization and stability phenomena in Li_2FeSiO_4 studied by PES/XPSic*, J. Mater. Chem. **16** (2006), 3483–3488.

[20] A.K. Padhi, K.S.Nanjundaswamy and J.B. Goodenough, *Phospho-olivines as Positive-Electrode Materials for Rechargeable Lithium Batteries*, J. Electrochem. Soc. **144** (1997), 1188–1194.

[21] G. Puglisia and L. Truskinovsky, *Rate independent hysteresis in a bi-stable chain*, Journal of the Mechanics and Physics of Solids **50** (2002) 165 – 187

[22] V. Srinivasan and J. Newman, *Discharge Model for the Lithium Iron-Phosphate Electrode*, Journal of The Electrochemical Society **151**(10) (2004), A1517–A1529.

[23] Srinivasan, V., Newman, J. *Existence of Path-dependence in the LiFePO4 Electrode*, Electrochem. Solid State Lett. **9** (2006), A110–A1529.

[24] M. Wagemaker, W.J.H. Borghols and F.M. Mulder, *Large Impact of Particle Size on Insertion Reaction. A Case for Anatase Li_xTiO_2*, J. AM. CHEM. SOC. **129**(14) (2007), 4323–4327.

[25] M. Wagemaker, A.P.M. Kentgens and F.M. Mulder *Equilibrium lithium transport between nanocrystalline phases in intercalated TiO_2 anatase*, Nature **418** (2002), 397–399.

[26] M. Wagemaker, F. M. Mulder and A. Van der Ven *The Role of Surface and Interface Energy on Phase Stability of Nanosized Insertion Compounds*, Advanced Materials **21** (2009), 2703–2709.

[27] A. Yamada, H. Koizumi, S.I. Nishimura, N. Sonoyama, R. Kanno, M. Yonemura, T. Nakamura and Y. Kobayashi *Room-temperature miscibility gap in Li_xFePO_4*, Nat. Mater. **5** (2006), 327–360.